Proceedings of the 9ICEG
9th International Congress on Environmental Geotechnics
25-28 June, 2023 | Chania, Greece
© Authors: All rights reserved, 2023
https://doi.org/10.53243/ICEG2023-41

Evaluation of ISS Sample Crusts formed During EPA 1315M Testing

D.G. Grubb[1], D.R.V. Berggren[2], R.W. Shannon[3], B.K. Schroth[4], C.D. Tsiamis[5] and J. Hess[6]

[1]Technology Fellow, Jacobs Engineering, Inc., 2001 Market Street, Suite 900, Philadelphia, PA, 19103, email: dennis.grubb@jacobs.com

[2]Technologist, Jacobs Engineering, Inc., 1100 NE Circle Blvd., Suite 300, Corvallis, OR 97330

[3] Laboratory Manager, Pittsburgh Mineral and Environmental Technology, 700 5th Ave, New Brighton, PA, 15066

[4]Principal Geochemist, Jacobs Engineering, Inc., 2485 Natomas Park Drive, Suite 600, Sacramento, CA 95833.

[5]Senior Project Manager, Chemical Engineer, US Environmental Protection Agency, 290 Broadway, New York, NY, 10007

[6] Project Manager, Jacobs Engineering, Inc., 500 7th Ave, New York, NY, 10018

ABSTRACT

Modified ("M") EPA 1315 tests have been used to assess the leaching of volatile organic compounds (VOCs) under simulated brackish water conditions to provide insight on mass transfer rates that result from in situ stabilization/solidification (ISS) of sediments at coastal sites heavily impacted by non-aqueous phase liquids (NAPLs). As verified in this study, the use of saltwater (SW) baths during EPA 1315M testing may result in the formation of surface crusts on ISS samples and mass transfer reductions of VOCs (and specifically naphthalene). Based on mineralogical analyses, the newly-formed ISS sample crusts (primarily aragonite and brucite) were similar in many respects to crusts formed on concrete under marine exposure conditions based on mineralogical analyses. Also verified was that the pH of the SW bath can drop from greater than 11 for a corresponding deionized (DI) water bath to approximately 8 during EPA 13135M testing, potentially enabling biological activity. However, while naphthalene degraders were detected in some tests, their impact on leaching behavior was not clear.

Keywords: Non-aqueous phase liquids, naphthalene, stabilization/solidification, leaching, seawater, aragonite

1 BACKGROUND AND CONTEXT

This paper builds on the stabilization/solidification (S/S) treatment of the non-aqueous liquid phase liquid (NAPL) impacted sediments in the Gowanus Canal, located in the Brooklyn Borough of New York City. The Gowanus Canal is a 1.8-mile (2.9 km)-long canal built in the 1860s that has been impacted by a combined sewer overflow (CSO) at the head of the canal (ongoing), and variety of historic industrial activities along its entire reach, including three former manufactured gas plants (MGPs) which are taken to be the primary source of NAPL impacts to the sediments. The Record of Decision (ROD) was issued in September 2013 (USEPA 2013) that called for the in situ stabilization/solidification (or ISS) of sediments in target areas with *potential for active upward NAPL migration from the native sediment,* that is, the "native alluvium" (or NA) positioned below the upper "soft sediment" (or SS), the latter of which will be removed and replaced with a reactive capping system. A series of papers detail the remedial investigation, design, in-canal ISS pilot, testing and delineation of ISS areas for treatment (Niemet et al 2014; Gentry et al 2014; Olean et al 2016; Grubb et al 2020; Gee et al 2022).

ISS in the uppermost reach of the canal (or Remedial Target Area 1; RTA-1) was completed in the Fall of 2022 using a minimum dose of 7.5 percent by dry weight (wt%) of a 60/40 (w/w) Type V Portland Cement (PC) / NewCem™ (NC) slag cement blend to the wet weight of the NA sediments for treatment depths up to 5 ft (1.5 m). Here, NewCem™ refers to Grade 120 ground granulated blast furnace slag (GGBFS). The specified ISS mix design also included 0.5 wt% powdered bentonite (B) and 0.1 wt% of an anti-washout solution (BASF UW450).

Figure 1 shows the RTA-1 ISS plan areas originally recommended for treatment (Gee et al. 2022), historic footprint of the Fulton MGP site abutting RTA-1, and the fresh ISS sample collection locations for this study (F-L-163; F-L-200). The yellow inset of Figure 1 provides an overview of the entire canal that was subdivided into three RTAs for project management purposes. Each turning basin (TB-#) is referenced by the numbered street with which it is aligned. Specifically, the ISS pilot (Olean et al 2016; Grubb et al 2020) was conducted in TB-7 located in RTA-2. The blue inset shows an expanded view of the fresh ISS sample collection, prior sediment (SED) and Tar-specific Green Optical Screening Tool (TarGOST®) borings locations.

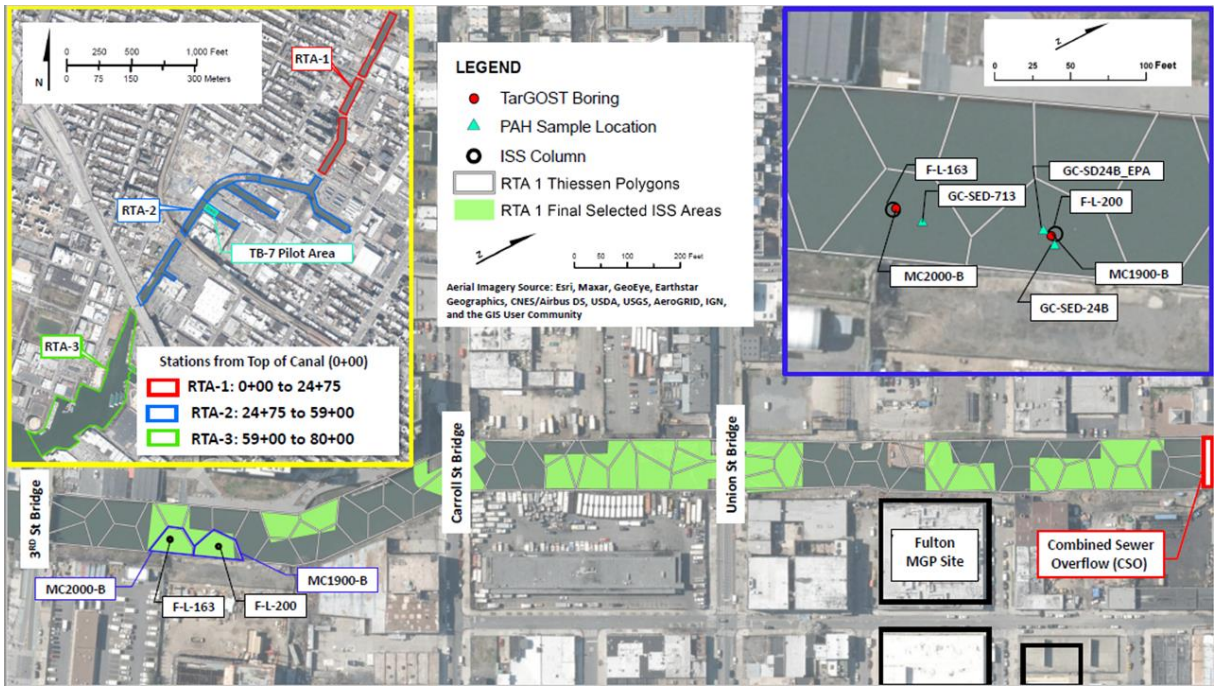


Figure 1. *Gowanus Canal Remedial Treatment Area 1 (RTA-1) showing ISS plan areas, ISS sample collection locations for the study (F-L-163, F-L-200) and general footprint of the historic "Fulton" Manufactured Gas Plant (MGP). (Aerial Imagery Source: Esri, Maxar, GeoEye, Earthstar Geographics, CNES/Airbus DS, USDA, USGS, AeroGRID, IGN, and the GIS User Community)*

The main motivation for this study stems from the observations of Grubb et al (2020) related to the apparent formation of "surface" crusts on the TB-7 ISS pilot samples during EPA 1315M leach testing under simulated brackish or saltwater (SW) conditions. Said crusts appeared to promote the reduced leaching of naphthalene by a factor of up to 10 versus the corresponding DI water leaching condition (no visible crusts). Grubb et al (2020) postulated that reactive calcium leaching from the ISS samples (Kitazume et al 2003) were reacting with the dissolved salts in the SW solution, buffering pH and creating new mineral precipitates on the ISS sample surface, effectively blocking the mass transfer of organic COCs such as naphthalene. Of note, the SW bath samples without visible surface crusts also had lower naphthalene leaching rates than the samples in DI water despite having similar dissolved organic carbon (DOC) mass transfer rates, the latter of which can aid the co-transport of petroleum hydrocarbons (EPRI 2009). This finding seemed to suggest that perhaps COC size mattered, and non-polar sterically complex COCs might be preferentially trapped by the crust materials.

For the SW bath exposed samples without visible crusts, it was hypothesized that because the NC is rich in amorphous silica and the SW bath pH values appeared to be titrating in and around the pKa (~9.5) of silicic acid (SiO_4), pore clogging may have occurred due to the formation of clear silicate (monomeric or polymeric) gels. This may have effectively sealed the surface, which would be consistent with their somewhat polished appearance in many cases. Thus, the organic COC leaching reductions were later apprehended to be independent of the visible appearance of a whitish or other colorized crust on the SW bath samples, which underscored the need to analyze the ISS sample surfaces. However, the pH of the SW baths was on the order of 8.5 to 10 versus pH > 11 for the DI water leaching conditions (see Fig 6a of Grubb et al 2020). The pH reductions were likely associated with the consumption of alkalinity during new mineral precipitation reactions, but more importantly, said pH reductions allowed

for the theoretical possibility that the SW baths became biologically active and biodegradation was responsible for the observed naphthalene reductions.

Accordingly, to assess if the ISS sample surface crusts and/or potential biodegradation were contributing to the apparent reductions in mass transfer of naphthalene during EPA1315M testing a study was developed to:

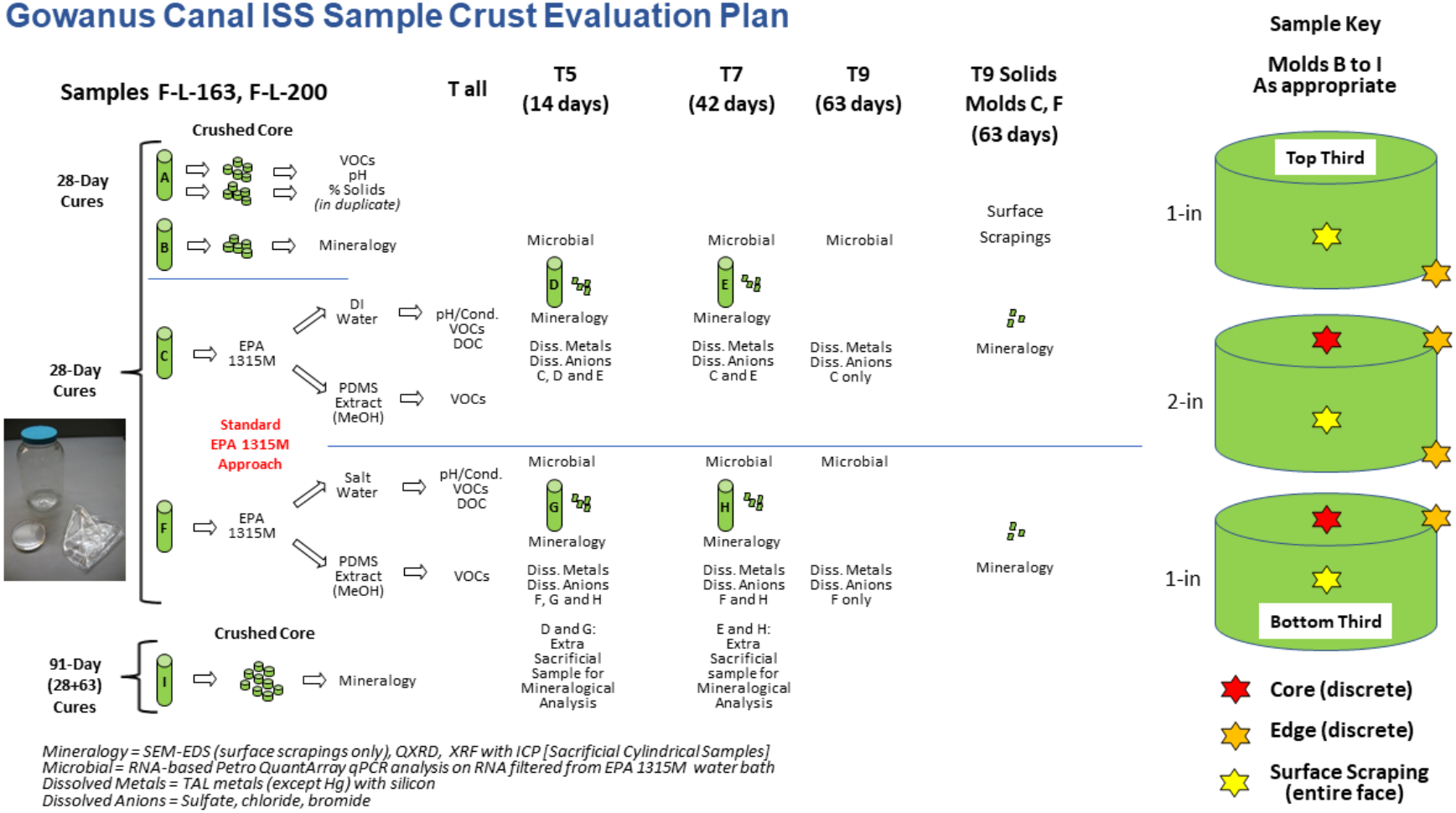
1) Reverify the potential for ISS crusts under SW bath conditions. This was accomplished using fresh ISS mix samples from RTA-1 and an approach generally consistent with the prior TB-7 ISS pilot (Grubb et al 2020). EPA 1315M testing was repeated on numerous 28-day cured samples under both DI water and SW bath conditions.
2) Mineralogically evaluate the nature of the leached ISS sample surfaces and their evolution with time versus their core composition (controls in sealed molds). Analysis techniques included optical microscopy (OM), quantitative X-ray powder diffraction (QXRD) using the Rietveld method, and X-ray fluorescence (XRF) with ICP to determine bulk chemistry and support QXRD interpretation, and scanning electron microscope energy dispersive X-ray spectroscopy (SEM-EDS). Note that soil-cement is a relatively friable material compared to concrete, precluding the preparation, staining and/or analysis of thin sections, etc., to assess the crust materials and/or biofilms on the ISS samples.
3) Quantify potential microbial activity in the DI water and SW baths as a function of time using gene probing techniques, specifically for benzene, toluene, ethylbenzene and xylene (BTEX), polynuclear aromatic hydrocarbons (PAHs), and other short chain petroleum hydrocarbon degraders.

Figure 2 illustrates the overall testing approach for the freshly collected ISS samples and cured in 5x10 cm (2x4 inch) sealable molds for a minimum of 28 days prior to testing. For the ISS crust evaluation, nine ISS sample replicates (A to I) were prepared. ISS sample Replicates A and B served as the controls. The central core and surface of Replicate B were both analyzed as shown in the exploded view of the molded sample (see Figure 2), as it was expected that the surface composition may not be representative of internal conditions due to boundary effects associated with the plastic mold during curing, including the accumulation of fines, mortar paste and potential NAPL along the perimeter. After 91 days of curing, Replicate I was analyzed in the same manner as Replicate B to illustrate potential changes in mineralogy associated with curing only (no water immersion).

28-day cured ISS sample Replicates C to H were submitted for EPA 1315M testing, in which the replicates were immersed in water for a testing period of up to 63 days (or a total of 91 days of ageing), with nine standard exchange intervals (denoted T1 to T9). Replicates C, D and E were tested under DI water bath conditions. Replicate C was analyzed for aqueous VOCs, pH, conductivity and DOC for all nine leaching intervals. Replicates D and E were operated in parallel to Replicate C, but without analysis of the water bath at every exchange point. Their testing was terminated at test interval T5 (14 days of leaching) and T7 (42 days), respectively, to enable mineralogical evaluations of the ISS sample surfaces (once dried), including cut edges to examine the thickness of potential ISS crusts (**Figure 2**). The corresponding water baths from the T5, T7 and T9 intervals were analyzed for dissolved major anions and cations, pH and conductivity (not reported here). A subsample of the Replicate C DI water bath was also filtered for RNA at these three time steps to document the activity of petroleum hydrocarbon degraders (functional gene copies), especially for naphthalene (see Grubb et al 2023 for discussion).

As summarized in Figure 2**,** Replicates F, G and H were tested in a parallel manner as Replicates C, D and F, but under SW bath conditions. Moreover, Figure 2 shows where mineralogical samples were collected from an individual monolithic ISS cylinder cut in three sections for ease of analysis. ISS edge and surface samples were both analyzed for their mineralogy. The sample nomenclature adopted for this analysis was *F-L-###_ "Replicate/Bath" _ "Interval" _ "Location."* For example, *F-L-200 SW T9 Edge* denotes the edge sample (for SEM-EDS) of Sample F-L-200 Replicate F at the end of the test (T9 = 63 days).

Gowanus Canal ISS Sample Crust Evaluation Plan



Mineralogy = SEM-EDS (surface scrapings only), QXRD, XRF with ICP [Sacrificial Cylindrical Samples]
Microbial = RNA-based Petro QuantArray qPCR analysis on RNA filtered from EPA 1315M water bath
Dissolved Metals = TAL metals (except Hg) with silicon
Dissolved Anions = Sulfate, chloride, bromide

2 MATERIAL AND METHODS

2.1 Field sample collection and curing

The F-L-163 and F-L-200 ISS column locations (Figure 1) were chosen as they were among the more MGP NAPL impacted locations in RTA-1 (Gee et al 2022). Fresh ISS samples were retrieved using an automated sediment sampler positioned at the mid-height of each ISS column before opening the sampler. After collection, the sediment sampler was sealed, brought to the surface, and placed directly over a flared top 20-gallon (77.5 L) HDPE container to release the fresh ISS materials. The fresh ISS materials were then subsampled and passed through a 9.5 mm (0.375-inch) sieve and placed in a series of 5x10-cm (2x4-inch) sealable molds. Individual mold samples were tamped during filling to liberate air bubbles. The mold tops were scraped level with a straight edge, the lids were closed, and the samples were placed upright in plastic bag with wet towelettes and sealed. All samples were then placed in a sealed cooler for humidity control and curing for 28-days prior to testing.

2.2 Baseline parameters

28-day cured samples (see Replicate A; **Figure 2**) were submitted for pH (EPA 9045D), moisture content (MC) by ASTM D2216 as well as total VOCs by EPA Methods 8260C since naphthalene and BTEX were of primary interest. Testing was completed in duplicate. Additional baseline data collected under the QA/QC program (B&B Engineers, 2022) included hydraulic conductivity (K) by ASTM D5084 using a confining pressure of 17.2 to 34.5 kPa (2.5 to 5 psi).

2.3 EPA 1315M Testing Suite

EPA 1315 semi-dynamic leach testing (EPA 2017a) was completed on S/S-treated soil samples cured for a minimum of 28 days based on their collection date. EPA 1315 was modified (M) and conducted in general accordance with EPRI (2009), Gentry et al. (2014) and Khuri et al (2022). The key modifications (M) included the use of zero headspace conditions and the addition of a PDMS coating on the inside walls of each leaching vessel (jar liner) to prevent dissolved hydrocarbons within the water bath from attaining their respective effective saturations during the leaching intervals (denoted T1-T9). Replicates C, D and E were placed in a DI water bath per the EPA 1315M method, while Replicates F, G, and H were placed in SW baths (Figure 2) containing Instant Ocean™ (Spectrum Brands; Blacksburg, VA) to simulated brackish water conditions with a salinity on the order of 28 g/L [or parts per thousand (ppt)], or approximately 80% of the typical ocean salinity (~35 ppt) (Millero et al 2008).

In either water bath, the PDMS serves as a strong sink for hydrocarbons, so the total mass leached from an ISS-treated sample during each interval is the sum of the COC mass in the water and PDMS (water+PDMS). After each exchange event, the sample surface was photographed, the water bath was removed, and the PDMS liner was extracted with methanol (30 mL) as recommended in EPRI (2009).

Water baths from Replicates C and F were analyzed for VOCs (EPA 8260D), dissolved organic carbon (DOC; SM 5310B), pH, and conductivity for all nine exchange events, while the methanol extract of the PDMS liner was submitted for VOC analysis by EPA 8260D. The water baths for Replicates D, E, G, and H were likewise exchanged, but were not analyzed except for the T5 (14 days) and T7 (42 days) intervals. At these two exchange events and T9 (63 days), each water bath was analyzed for dissolved major anions and cations (EPA 6010C/300.0), pH, and conductivity. The T5, T7, and T9 water baths from Replicates C and F were also subsampled and filtered for analysis of RNA activity.

Side-by-side photographs of the C and F replicates were taken for each sample series prior to re-immersion in the replacement water bath. Testing was terminated for Replicates D and G at T5, and Replicates E and H at T7 to provide ISS sample solids for mineralogical testing. Replicates C and F were also provided for mineralogical testing after completion of the test at T9.

2.4 Mineralogical Suite

ISS sample Replicates B and I were first cut into three pieces (while still in their sample molds) measuring approximately 2.5-, 5- and 2.5-cm (1-, 2- and 1-inches) a tile saw then oven dried at 70°C for 48 hours to eliminate free moisture and to eliminate ongoing carbonation reactions. Replicates C to H (wet from EPA 1315M testing) were first oven-dried prior to cutting and/or subsampling.

Each replicate was then sequentially subsampled to produce “core,” “edge,” and “surface” samples as illustrated in Figure 2. First, a small Dremel 4000 electric saw (Racine, WI) with a wafer blade was used to obtain *core* samples from the geometric center of each internal cut face (diameter) of the ISS mass replicate. Second, *edge* samples were then collected from (chipped off) the perimeter of the ISS mass cylinder where it intersected the sidewall for SEM-EDS analyses. In a similar fashion, discrete *surface* samples were obtained from the sidewalls of the ISS mass for SEM-EDS. Lastly, the circumferential surface of the three ISS sections were then gently scraped by hand using a 3-inch (7.5 cm) steel box cutter blade to remove the perimeter surface (sidewall) deposits for analysis. Sufficient mass of *core* and *surface* materials were collected to enable QXRD, XRF and SEM-EDS analyses. For *edge* and select *surface* samples, a few chipped fragments from each replicate were retained for SEM-EDS analyses.

For compositional analyses (XRD, XRF), each ISS core and surface sample was crushed and passed through a No. 70 sieve (210 µm). The materials passing the No. 70 mesh were split using a riffle splitter to obtain a 30-gram aliquot. These analytical aliquots were then pulverized and sieved through a No. 200 screen (74 µm) for XRF/ICP analysis and then a split was pulverized again to pass a No. 400 sieve (37 µm) for XRD analysis. For brevity, the elemental composition, quantitative x-ray powder diffraction using the Rietveld method (1969) and standard SEM-EDS procedures.

3 RESULTS AND DISCUSSION

Table 1 summarizes the environmental baseline parameters of the fresh ISS samples used in this study. The pH of the samples was 12.5 based on a L/S of 1 with average total naphthalene content of approximately 1,345 mg/kg (F-L-163) and 2,465 mg/kg (F-L-200). These values are very representative of the average conditions in RTA-1 (Gentry et al 2014) and consistent with the untreated NA sediment samples tested during the TB-7 ISS pilot, where 9 of 10 samples had naphthalene contents between 187 and 2,860 mg/kg with a median value of 1,320 mg/kg by EPA 8260C (Grubb et al 2020).

Table 2 shows the results from K (ASTM D5084) testing on QA/QC samples collected in parallel with the F-L-163 and F-L-200 leaching samples, including the reported MC and dry bulk density (DBD) values. The MCs were fairly similar, but the F-L-163 samples were slightly denser by about 3 lb/ft^3 (0.47 kN/m^3). The F-L-163 sample was approximately 40 times less permeable than the F-L-200 sample. For comparison, Table 2 shows the comparable mix designs from the TB-7 pilot (Grubb et al 2020) that used the same (7.5 wt%) and 2.5 wt% higher (10 wt%) cement blend doses. The TB-7 samples were denser at the same 7.5 wt% dosing level. The K values for the TB-7 ISS pilot mixes were comparable to slightly greater than the F-L-163 samples.

3.1 EPA 1315M Results

Figure 3 shows the EPA 1315M naphthalene water bath concentrations and cumulative mass release (CMR) curves for the F-L-163 and F-L-200 (Replicates C and F) in comparison to the prior TB-7 ISS pilot results. Note that Figure 3a contains only the water concentrations, they are not effective concentrations (water+PDMS that accounts for the mass accumulated in the PDMS jar liner). In Figure 3a, the naphthalene DI water bath concentrations show that the measured concentrations are not very sensitive to changes in blended cement dose consistent with other EPA 1315M leaching studies (Gentry et al 2014; Grubb et al 2020; Khuri et al 2022). Also, the SW bath concentrations for F-L-163 and F-L-200 only differ by a factor of 2 to 3 from the DI water bath data toward the end of the respective tests, in contrast to the TB-7 data pairs, where the difference can exceed an order of magnitude. The total mass released from the sample (water+PDMS) is accounted for in the CMR curve (Figure 3b).

Table 1. *Environmental Baseline Parameters for 28-day Cured ISS samples (detected compounds only)*

	F-L-163		F-L-200	
Analyte	**Rep 1**	**Rep 2**	**Rep 1**	**Rep 2**
Percent Moisture (%)	28.9	29.6	37.3	38.7
pH (S.U.)	12.4	12.4	12.3	12.4
Volatile Organic Compounds by EPA SW8260C (mg/kg)				
cis-1,2-Dichloroethene	0.766 U	0.486 U	5.6	6.64
Ethylbenzene	26.2	26.3	42	39.4
Isopropylbenzene (Cumene)	6.71	7.08	9.97	9.42

m&p-Xylene	2.46	U	8.88	23.3	21.5
Naphthalene	1,340		1,350	2,560	2,370
o-Xylene	11.9		11.9	18.6	17.1

All data in mg/kg dry solids.
U – indicates the analyte was analyzed for but not detected above the method detection limit (MDL). MDL is reported.

Table 2. *Summary of Geotechnical Parameters for 28-day Cured ISS samples*

		F-L-163	F-L-200	GC7.5B (C253)	GC10B (C239)
Reagent Dose					
PC	wt%	4.5	4.5	4.5	6.0
NC	wt%	3.0	3.0	3.0	4.0
Bent.	wt%	0.5	0.5	0.5	0.5
W/R	mL/g	1.4	1.4	1.4	1.4
ASTM D5084					
MC_{final}	%	39.5	42.8	36	32.3
S_{final}	%	95.1	95.2	98	99
DBD	lb/ft3	76.7	73.4	82.2	87.1
K	cm/s	9.7E-07	3.8E-06	1.5E-06	2.1E-06
EPA 1315M					
$MC_{ave,\ totals}$	%	29.3	38.0	34.1	26.1
DBD	lb/ft3	85.1	73.8	79.8	90.0

GC denotes TB-7 pilot (Grubb et al 2020). Reagent doses reported on a weight percent (wt%) basis of wet sediment
W/R = final water-to-dry reagent ratio at mixing; mL/g = millilitres per gram
MC_{final} = final moisture content
S_{final} = final degree of saturation
DBD = dry bulk density; lb/ft^3 = pounds per cubic foot
K = permeability measured at 20°C and effective stress of 2.5 to 5 lb/in^2; cm/s = centimetres per second

Figure 4 shows the pH and DOC CMR curves for the EPA 1315M tests. As expected, **Figure 4a** shows that the pH data for the DI water bath samples from the Gowanus Canal are tightly clustered by leaching interval since the blended cement dose only differs by 2.5 wt%. All pH values are greater than 11, and the F-L-200 data plots incrementally higher than F-L-163. The SW bath data (open symbols) for the TB-7 data shown in Figure 4a reflect differences in cement doses, and the RTA-1 plot between these data. Interestingly, the F-L-200 SW sample data plots substantially higher than F-L-163 for the same dosing

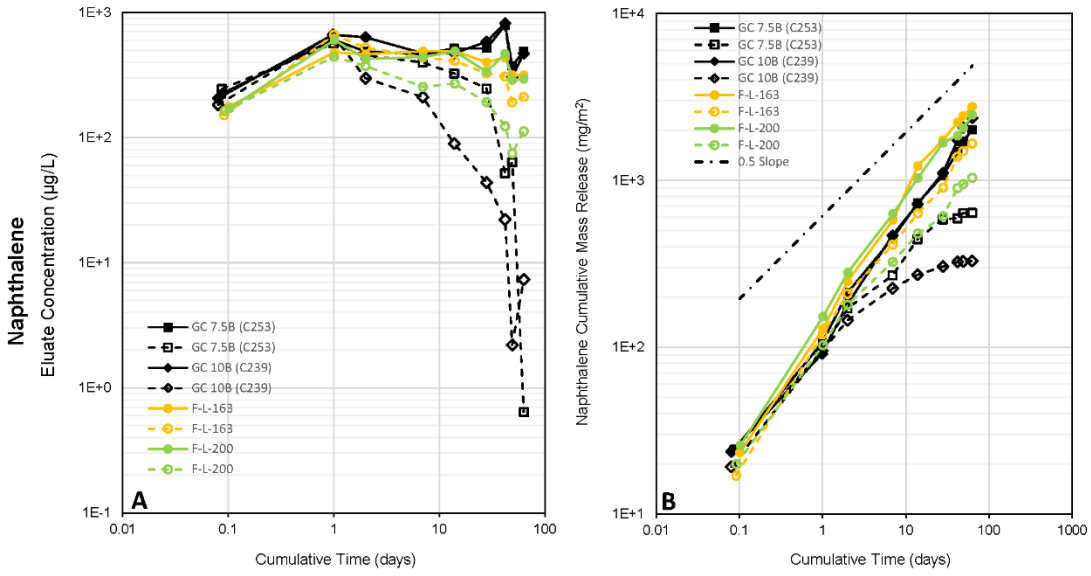


Figure 3. *EPA 1315M naphthalene leaching bath concentrations (A) and cumulative mass release (B) of ISS-treated samples the site. DI and SW leaching bath conditions denoted by solid symbols and lines, and open symbols and dashed lines, respectively.*

rate, perhaps owing to its greater ability to release alkalinity (40x higher K, see Table 2) and/or less buffer capacity associated with the sediment solids despite F-L-163 being slighter denser and therefore

containing a greater total mass of cement. Based on the pH trends shown in Figure 4a, it was expected that below approximately pH~9, the potential for microbial activity increased significantly, leading to the obvious concern that the measured naphthalene concentrations were biologically reduced since no biocide (e.g. sodium azide) was deployed in any of the EPA 1315M tests due to safety considerations. The DOC CMR curves (Figure 4b) suggested that the SW bath conditions may be associated with 50% reduction in DOC transport. This general trend would be consistent with the observation of the crusts in the GC samples.

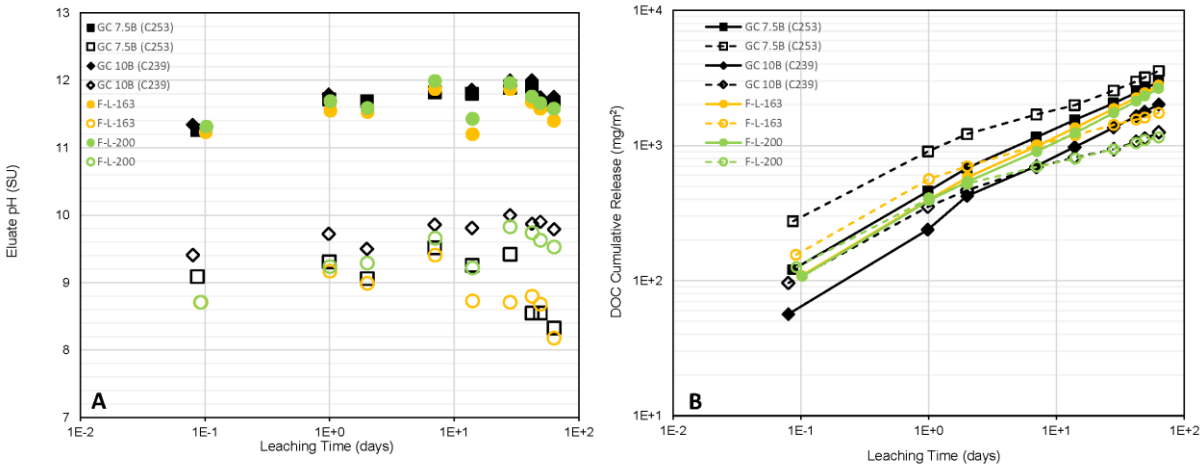


Figure 4. *USEPA 1315M pH (A) and DOC cumulative mass release (B) for the site. DI and SW leaching bath conditions denoted by solid symbols and lines, and open symbols and dashed lines, respectively.*

3.2 Mineralogical Results

For brevity of presentation, the discussion will focus on the F-L-200 samples, as the quantitative results and images for F-L-163 were comparable, but more muted. The QXRD results for the PC blend, 28- and 91-day controls (Replicates B, I) and EPA 1315M DI water and SW bath samples (Replicates C to F) are presented in Table 3. As expected, the PC blend was dominated by calcium/magnesium silicates [hatrurite (or C3S in cement nomenclature), larnite (C2S), merwinite, and periclase] as well as brownmillerite and various polymorphs of calcium sulfate (gypsum, bassanite and anhydrite). The amorphous content was approximately 52%.

After PC blending and curing with the NA sediments, the mineralogy of the ISS mix designs was dominated by aluminosilicate minerals, chiefly, quartz, albite, mica and potassium feldspar likely derived from the sediments. Carbonation products included hydrotalcite, calcite and dolomite. Oddly, portlandite was detected in the 28-day samples as curing reactions were ongoing but was not detected in the raw PC blend and was all but expended by 91 days curing. Otherwise, the core and surficial compositions for the 28- and 91-day cured samples were very similar except that the surficial samples typically had 3 to 4 more wt% of amorphous content, likely attributed to sample boundary effects with the plastic mold (which appeared to primarily dilute the quartz fraction).

Figure 5 shows photographs of the F-L-200 DI water and SW baths samples immediately after removal from the bath at test termination (T9), patted dry with papers towels to remove excess water (a); in an air-dried condition (~20 hrs) (d); and at magnification levels of 3x and 30x for the respective interest areas for the air-dried DI water (b,e) and SW bath (c,f) samples. The dense coverage of new precipitates on the ISS sample surfaces is shown in **Figure 6** for the T9 surface samples, respectively. **Figure 6a** shows a top view of spherulitic and/or radial aragonite crystals comprised of individual nano-rods (Figures 6c,d) of aragonite consistent with those reported by Giampouras et al (2020). Since Mg interferes with calcite precipitation, aragonite emerges the preferred polymorph of $CaCO_3$ in seawater (Buenfeld and Newman 1986; Sabbides et al 1992).

Table 3 shows the pH and mineralogy of the DI water and SW bath samples ordered by interval. The surficial mineralogy of the T5 to T9 samples barely changed, except that the amorphous content monotonically increased by 8 wt% with time, largely at the expense of quartz since all other minerals underwent minor fluctuations. No tricalcium aluminate (C3A) was detected in the PC blend and the Al_2O_3

Table 3. *Quantitative X-Ray Powder Diffraction Results Summary for F-L-200 samples*

			Mold Samples[b]									
			B		I		D	E	C	G	H	F
		PC blend[a]	Control		Control		DIW	DIW	DIW	SW	SW	SW
Mineral	Formula	N/A	Core 28 day	Surf. 28 day	Core 91 day	Surf. 91 day	Surf. T5	Surf. T7	Surf. T9	Surf. T5	Surf. T7	Surf. T9
pH[c]							11.43	11.76	11.58	9.22	9.74	9.53
Hatrurite	$Ca_3(SiO_4)O$	23.70										
Larnite	Ca_2SiO_4	12.80										
Brownmillerite	$Ca_4Al_2Fe_2O_{10}$	4.60										
Merwinite	$Ca_3Mg(SiO_4)_2$	2.80										
Gypsum	$CaSO_4 \cdot 2H_2O$	1.50	0.40	0.40	0.50	0.80				1.10	0.90	
Bassanite	$CaSO_4 \cdot 0.5H_2O$	1.10	0.10	0.30						0.90	0.50	0.40
Anhydrite	$CaSO_4$								0.40			
Periclase	MgO	1.20										
Quartz	SiO_2	0.20	39.40	32.00	39.80	36.90	41.91	38.80	35.80	33.90	30.50	27.00
Albite[d]	$(0.75Na,0.25Ca)AlSi_3O_8$		8.70	10.90	10.00	8.70	9.89	8.50	8.50	7.20	8.40	7.30
Mica	$KAl_2(Si_3Al)O_{10}(OH)_2$		6.10	7.00	5.30	5.70	5.42	4.60	5.50	3.30	3.60	5.40
K-feldspar	$KAlSi_3O_8$		4.10	2.70	4.90	3.30	3.41	4.00	3.40	4.50	3.60	3.90
Chlorite	$(Mg,Al,Fe)_6(Si,Al)_4O_{10}(OH)_8$		1.30	3.60	1.80	0.90	1.13	1.30	1.30	1.60	2.40	2.00
Horneblende	$CaMg_2Fe_2Al(Si_7,Al)O_{22}(OH)_2$		1.40	1.10	1.60	1.90	0.26	0.60	0.80	1.10	1.40	1.50
Kaolinite	$Al_2Si_2O_5(OH)_4$		1.30	1.40	1.60	1.20	1.34	1.50	1.10	1.10	0.90	1.10
Hydrotalcite	$Mg_6Al_2(CO_3)(OH)_{16} \cdot 4H_2O$		2.00	1.80	2.20	2.20			0.60	1.10	1.20	1.00
Calcite	$CaCO_3$		1.70	2.60	1.30	1.70	4.84	4.20	3.10	2.80	2.10	1.20
Aragonite	$CaCO_3$									**3.50**	**7.20**	**8.80**
Dolomite	$CaMg(CO_3)_2$		1.10	1.20	0.90	2.20	0.91	0.70	0.90	1.20	0.40	0.80
Nordstrandite	$Al(OH)_3$											
Portlandite	$Ca(OH)_2$		0.70	0.90		0.20			0.20			
Brucite	$Mg(OH)_2$									**5.30**	**6.80**	**6.10**
Sjoegrenite	$Mg_6Fe_2(CO_3)(OH)_{16} \cdot 4H2O$						**0.42**	**0.30**		**0.10**	**0.30**	**1.00**
Halite	NaCl									**0.50**	**0.60**	**1.40**
Iron	Fe		0.10			0.20	0.19	0.20	0.10	0.20	0.10	
Amorphous		52.20	31.80	34.20	30.20	34.20	30.30	35.30	38.20	30.70	29.20	31.10
	TOTAL	100.1	100.2	100.1	100.1	100.1	100.0	100	99.9	100.1	100.1	100

All data in dry weight %.[a] PC blend: 7.5 wt% 60/40 Type V PC / NC with 0.5 wt% bentonite for a total of 8 wt% added to wet weight of sediment.
[b] Bold lettered quantities denotes new surface minerals. [c] pH data from EPA 1315M water bath analyses. See Figure 3. [d] (0.25Ca) basis

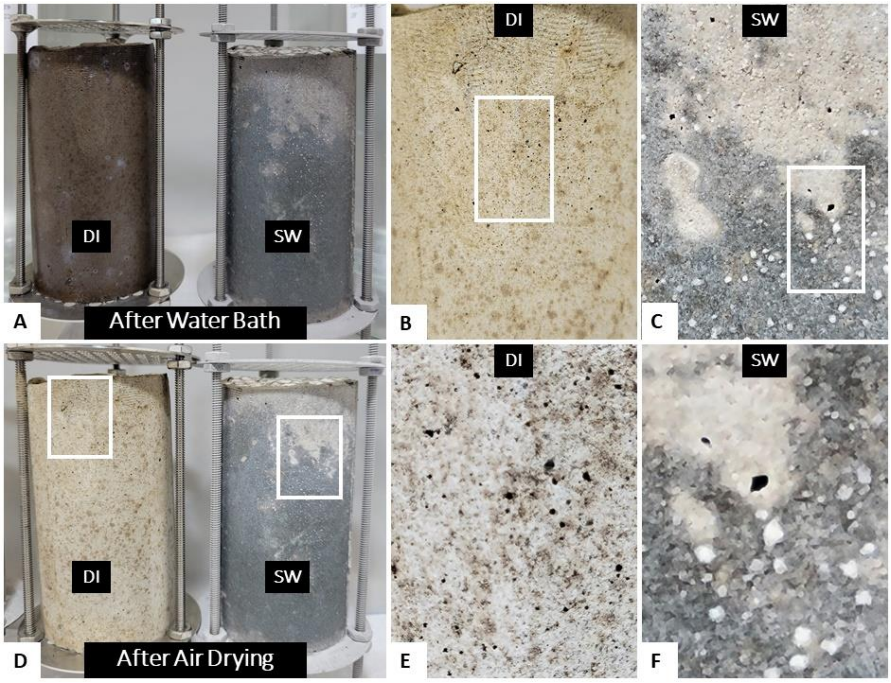


Figure 5. *Photographs of F-L-200 T9 mold samples immediately after EPA 1315M test completion with pat drying to remove excess surface water (A) and after minimum of 24 hours air-drying (B). Zoom shots (3x and 30 magnification) of the air-dried DI water (B,E) and SW (C,F) ISS sample surfaces. Visible crusts dominated SW samples (halite crystals are large white deposits). Dashed inset boxes show interest areas for subsequent magnification level.*

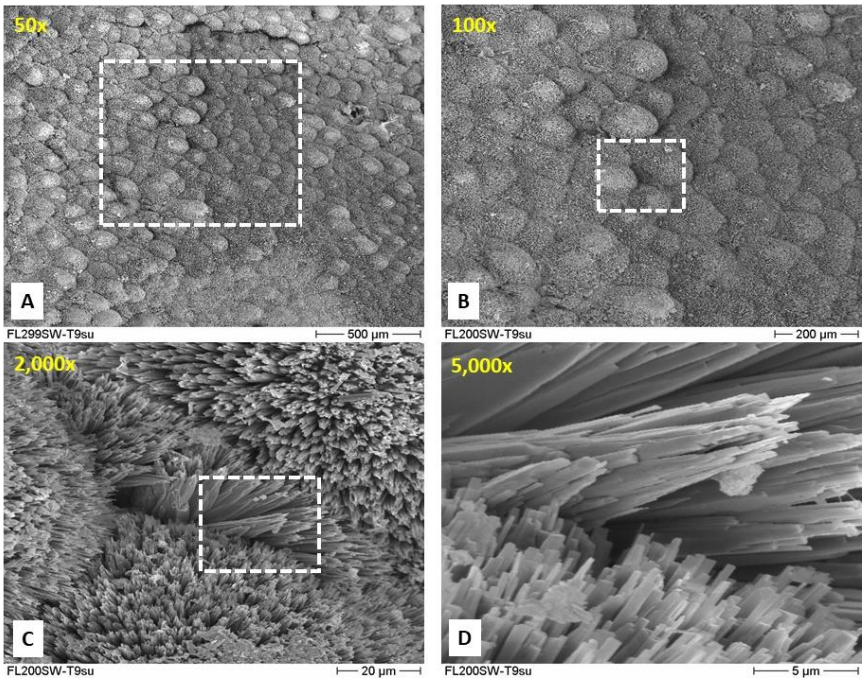


Figure 6. *SEM-EDS images of F-L-200 SW T9 surface samples at four magnification levels revealing dense packing and clustering of spherulitic and/or radial aragonite crystals (A,B) comprised of individual nano-rods of aragonite (C,D). Dashed inset boxes show interest areas for subsequent magnification level.*

content of the PC blend was very low (6.6 wt%). When applied to the NA sediments at an overall reagent dose of 7.5 wt%, the PC blend did not likely provide enough free Al to the system to enable sufficient ettringite [$Ca_6Al_2(SO_4)_3(OH)_{12} \bullet 26H_2O$] formation above detectable concentrations, either in the internal core or the surface of the ISS samples. As such, reaction outcomes related to ettringite

[$Ca_6Al_2(SO_4)_3(OH)_{12} \bullet 26H_2O$], Friedel's [$Ca_2Al(OH)_6(Cl,OH) \bullet 2H_2O$] and/or Kuzel's [$Ca_4Al_2(SO_4)_{0.5}Cl(OH)_{12} \bullet 6H_2O$] salt formation in/on the surface of the ISS samples were likely mitigated in comparison to concrete systems under marine exposure conditions (see for example, De Weerdt et al 2014; Park et al 2021). Additionally, hydrotalcite was observed in the both the controls and SW bath sample surfaces and may have acted as a sink for soluble Al. However, it was not observed in 5 of 6 DI water bath sample crusts.

A new carbonation product was detected in the T5 and T7 DI water surficial samples (sjöegrenite), signaling the dissolution of Fe (from ISS solids) and re-precipitation with Mg. Sjöegrenite was also detected in the SW bath samples (Replicates F to H), as were three other minerals exclusive to the SW baths: aragonite, brucite and halite (white crystals in **Figures 5c** and **f**). Their amounts generally increased with time while the amorphous content was essentially unchanged. Interestingly, when Replicates F (91-day cured SW surface) and I (91-day core) are compared, the loss of the quartz (~12%) and albite (~3%) contents in the SW bath samples match the emergence of aragonite (~9%) and brucite (~6%), except neither of the two new precipitated species contain alumina, potassium or silica. Instead, the occurrence of brucite and aragonite as new ISS crust materials is consistent with the observations of Buenfeld and Newman (1986) who observed rapid forming two-layered brucite/aragonite coatings on concrete samples in marine applications. Buenfeld et al (1986) reported that said brucite layer tend to densify the interfacial region via pore clogging, based on resistivity measurements. De Weerdt et al (2016) and Fjendbo et al (2022) similarly reported that the concrete/saltwater interfacial region also densified based on UV/fluorescent OM, capillary suction and porosity experiments but did not specifically limit this pore clogging effect to brucite.

Figure 7 shows SEM images at two scales for the F-L-200 ISS T9 edge samples immersed in DI water (a,c) and SW (b,d). No discernable crusts were observed on the T9 edge samples from the DI water bath, although it appears that localized dissolution and re-precipitation resulted in a "dusting" of new minerals, likely including various calcium silicates and calcite/aragonite. Conversely, the T9 edge samples from the SW bath (Figures 7b,d) show dense coverage by spherulitic and/or radial aragonite crystals (Buenfeld and Newman 1986; Giampouras et al 2020) with a thickness on the order of 45 µm. Interspersed with the aragonite are visible euhedral hexagonal crystals of varying size typical of brucite (Rausis et al 2020; Giampouras et al 2020).

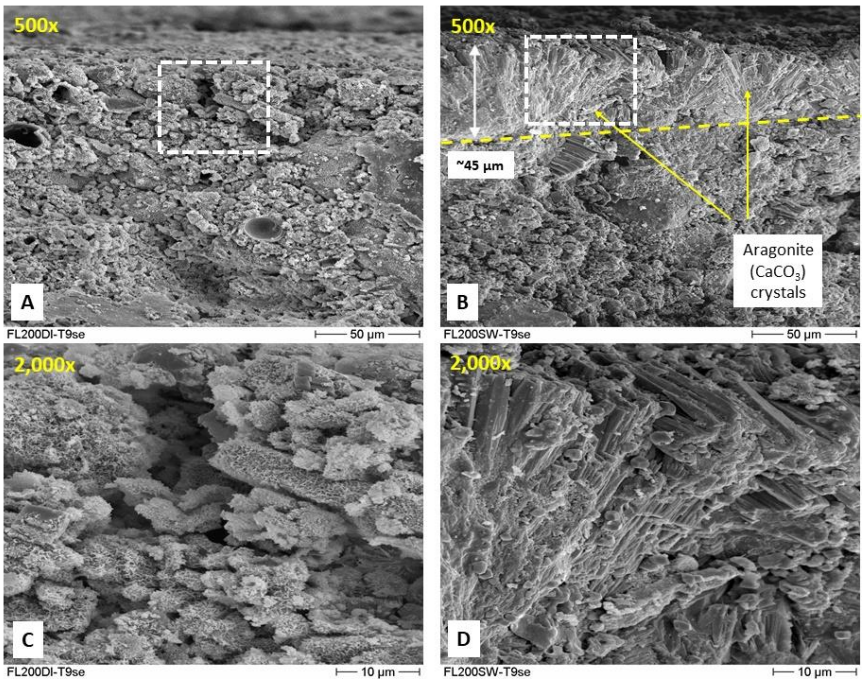


Figure 7. *SEM-EDS images of F-L-200 T9 edge samples at two magnification levels. DI water bath samples (A,C) reveal no discernable crust, only minor dusting of redistributed minerals. SW bath samples show densely packed crust with distinct, radially-shaped aragonite crystals (B,D) approximately 45 um in thickness interspersed with euhedral hexagonal crystals of brucite (D). Dashed inset boxes show interest areas for subsequent magnification level.*

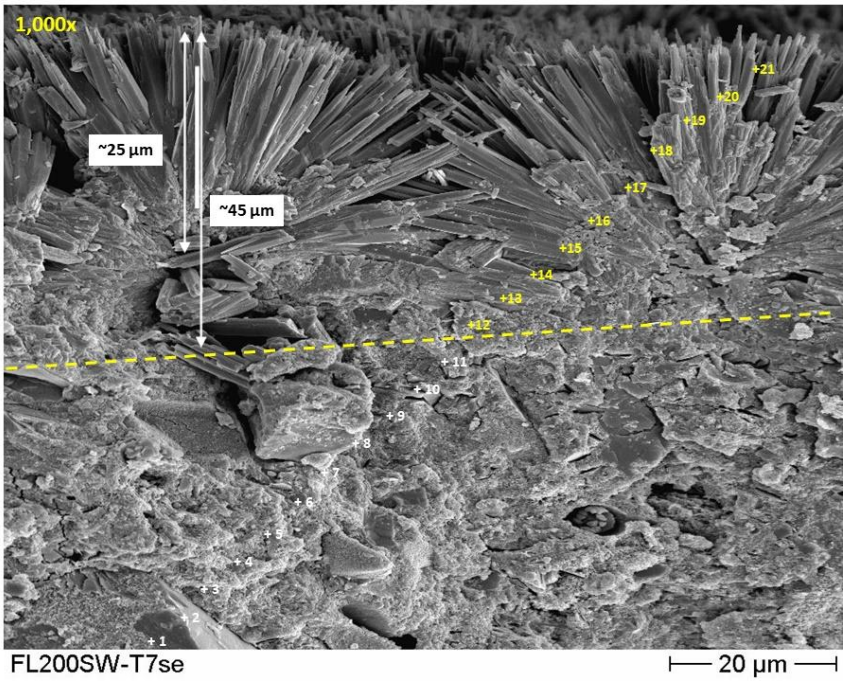


Figure 8. *SEM-EDS image of F-L-200 SW T7 edge sample and EDS point analysis targets that shows a densely packed upper crust (EDS points 12 to 21) with distinct, radially-shaped aragonite crystals approximately 25 to 45 µm in thickness. Deeper crust layer (EDS points 1 to 11) is enriched in magnesium well above ISS core composition (1.04% normalized elemental). See Table 5 for corresponding EDS data.*

The radial aragonite crystals are more distinct in Figure 8, which shows an enlarged SEM image of the T7 edge sample from the SW bath including 21 EDS point analysis locations. Table 4 presents the corresponding EDS results. Aside from some minor detections of Na, Mg, and Si, Figure 8 shows that the upper ISS surface crust is highly enriched in calcium (>90%) (C and O not reported) and is on the order of 25 to 45 µm in thickness before the EDS results transition to a significantly Mg-enriched zone, presumed to be brucite based on XRD analyses (Table 3) and elevated pH internal to solid. To be sure, the 91-day cured F-L-200 core materials contained only 1.04 wt% Mg on a normalized elemental basis with 100% of this mass committed to the phases shown in Table 3. Moreover, since C3A was absent from the PC blend used here and the Al elemental content was very low, the ISS crust layering observed in this work appears generally consistent with Buenfeld and Newman (1986) rather than the thaumasite, ettringite and Friedel's/Kuzel's salt dominated outcomes observed by De Weerdt et al (2014) and Park et al (2019) for their concrete specimens and simulations, respectively.

In summary, Figures 5 to 8 show extensive ISS sample crust coverage that can easily be on the order of 25 to 45 µm thickness within 63 days of exposure. Borrowing from the cement/concrete literature, the coupled aragonite surface layer (with brucite rich layer below) has the potential to directly reduce the mass transfer of naphthalene in two main ways: 1) via significant pore clogging of the near surface of the ISS sample by brucite and other minerals with time; and 2) by increasing the total thickness of the ISS sample via new surface precipitates, and thus the diffusion distance for organic COCs. Pore clogging phenomena at the cement/concrete surface has been verified by several researchers (Buenfeld et al 1986; De Weerdt et al 2016; Fjendbo et al 2022) and similar minerals have been observed in the Gowanus Canal soil-cement samples. Buenfeld et al (1986) also reported that aragonite layers can be upwards of 150 µm on concrete mortar samples after 120 days of saltwater exposure. Thus, it is likely that longer term EPA 1315M tests will correspond to thicker ISS samples crusts. As such, and without consideration of biological factors, the use of SW baths alone in EPA 1315M testing has the ability to change (lower) the trajectory (slope) of the naphthalene (and other organic COC) CMR curves as observed in Figure 3b.

4 CONCLUDING REMARKS

The goal of this study was to evaluate the ISS crusts under EPA 1315M SW leaching bath conditions to understand the mineralogical nature of the ISS crusts, to evaluate biological activity, and the potential role of both on the observed naphthalene reductions. The key observations include:

- The presence of mineral crusts was reconfirmed in the GC ISS samples immersed in EPA 1315M SW baths. Crust formation was rapid, with most of the original ISS surface obscured by 14 days (T5 interval). QXRD and SEM-EDS confirmed that the main crystalline minerals comprising the new crust were aragonite, brucite and sjöegrenite. The uppermost portion of this crust was dominated by aragonite (25 to 45 µm), the lower portion dominated by brucite, largely consistent with the surface evolution of concrete samples observed by Buenfeld and Newman (1986). The GC ISS samples in the DI water bath had no discernable crusts as determined by QXRD and SEM-EDS, however a fine "dusting" of the outer surface was noted, but its composition could not be assessed.
- The use of 60/40 Type V PC / SC blend corresponded to a low Al_2O_3 content of the PC blend (6.6 wt%). When applied to the NA sediments at an overall reagent dose of 7.5 wt%, it did not likely provide enough free Al to the system to enable sufficient ettringite formation above detectable concentrations, either in the internal core or the surface of the ISS samples. This likely also suppressed or obviated the formation of Friedel's/Kuzel's salts on the ISS surface, and thus the results observed here represent a departure from the surface evolution observed in traditional cement mortar/concrete saltwater exposure tests. Hydrotalcite was observed in both the controls and the SW bath sample surfaces and may have acted as a sink for soluble Al, however, it was not observed in 5 of 6 DI water bath sample crusts.
- Overall, the aragonite crusts appeared very densely packed by the end of the EPA 1315M test, appearing to contribute to the lower mass transfer rates of the naphthalene in the SW baths. The combination of pore clogging (lower K) near, and new precipitates (increased diffusion distance) on the ISS sample / saltwater interface can thus change (lower) the CMR slope from DI water conditions. That said, the naphthalene leaching results observed here under SW bath conditions were more muted than observed for the prior TB-7 ISS pilot (Grubb et al 2020).
- The bacterial assay work conducted on GC soil-cement samples from the EPA 1315M tests was confounding, see Grubb et al 2023 for full discussion. There was no clear evidence that specific or general potential biological activity occurring in the SW baths produced a meaningful effect on naphthalene mass transfer. Bacterial populations were increasingly encountered in the later stages of the EPA 1315M test (e.g. T9), even in the DI water bath. As such, longer duration EPA 1315M tests with additional -7 and/or 14-day leaching intervals out to 120 days, for example, may require additional scrutiny and testing, and is an area of future study.

REFERENCES

B&B Engineers & Geologists of New York. 2022. *RTA1 ISS – Results for sampling of F-L-163 and F-L-200,* Pennington, NJ, May.

Buenfeld, N. R., and J.B. Newman. 1986. The development and stability of surface layers on concrete exposed to sea-water. *Cement and Concrete Research*, *16*(5), 721-732.

Buenfeld, N. R., Newman, J. B., and C.L. Page. 1986. The resistivity of mortars immersed in sea-water. *Cement and concrete Research*, *16*(4), 511-524.

De Weerdt, K., Justnes, H., and M.R. & Geiker. 2014. Changes in the phase assemblage of concrete exposed to sea water. *Cement and Concrete Composites*, *47*, 53-63.

De Weerdt, K., Orsáková, D., Müller, A. C., Larsen, C. K., Pedersen, B., and M.R Geiker. 2016. Towards the understanding of chloride profiles in marine exposed concrete, impact of leaching and moisture content. *Construction and Building Materials*, *120*, 418-431.

Electric Power Research Institute (EPRI). 2009. *Leaching Assessment Methods for the Evaluation of the Effectiveness of In Situ Stabilization of Sediment Material at Manufactured Gas Plan Sites, EPRI and Exelon Corporation, First Energy Corporation and Southern Company, Palo Alto, CA, 1015553.*

Fjendbo, S., Sørensen, H. E., De Weerdt, K., Jakobsen, U. H., and M.R. Geiker. 2022. Correlating the development of chloride profiles and microstructural changes in marine concrete up to ten years. *Cement and Concrete Composites*, 104590.

Gee, G. L., Grubb, D. G., Gentry, J. L., Tsiamis, C. D., and J. Hess. 2022. Gowanus Canal Superfund Site. IV: Delineation of Potentially Migrating NAPL Layers for ISS Treatment. *Journal of Hazardous, Toxic, and Radioactive Waste*, *26*(3), 04022020.

Gentry, J. L., Niemet, M. R., Grubb, D. G., Bruno, M., Berggren, D. R., and C.D. Tsiamis. 2014. Gowanus canal superfund site. II: stabilization/solidification of MGP-impacted sediments. *Journal of Hazardous, Toxic, and Radioactive Waste*, *19*(1), C4014004.

Giampouras, M., Garrido, C. J., Bach, W., Los, C., Fussmann, D., Monien, P., and J.M. García-Ruiz. 2020. On the controls of mineral assemblages and textures in alkaline springs, Samail Ophiolite, Oman. *Chemical Geology*, *533*, 119435.

Grubb, D. G., Himmer, T. M., Gentry, J. L., Salter-Blanc, A. J., and C.D. Tsiamis. 2020. Gowanus Canal Superfund Site. III: Leaching of In Situ Stabilization/Solidification Mix Designs. *Journal of Hazardous, Toxic, and Radioactive Waste*, *24*(4), 04020045.

Khuri, R. E., Berggren, D. R., and D.G. Grubb. 2022. EPA LEAF Testing of Chlorobenzene-Impacted Sands and Soil–Cement Mix Designs. *Journal of Hazardous, Toxic, and Radioactive Waste*, *26*(3), 04022019.

Kitazume, M., Nakamura, T., Terashi, M., and K. Ohishi. 2003. Laboratory tests on long-term strength of cement treated soil. In *Grouting and ground treatment* (pp. 586-597).

Millero, F. J., Feistel, R., Wright, D. G., and T.J. McDougall. 2008. The composition of Standard Seawater and the definition of the Reference-Composition Salinity Scale. *Deep Sea Research Part I: Oceanographic Research Papers*, *55*(1), 50-72.

Niemet, M. R., Gentry, J. L., Bruno, M., Berggren, D. R., and C.D. Tsiamis. 2014. Gowanus Canal Superfund site. I: NAPL mobility testing of MGP-impacted sediments. *Journal of Hazardous, Toxic, and Radioactive Waste*, *19*(1), C4014003.

Olean, T.J., Gentry, J.L., Salter-Blanc, A.J., Himmer, T.M., Bruno, M. and C.D. Tsiamis. 2016. "In-Canal Stabilization/Solidification of NAPL-Impacted Sediments." *Remediation Journal*, *26*(3).

Park, S., Suh, Y., Nam, K. H., and Y. Won. 2021. Thermodynamic Modeling of Long-Term Phase Development of Slag Cement in Seawater. *KSCE Journal of Civil and Environmental Engineering Research*, *41*(4), 341-345.

Sabbides, T., Giannimaras, E., and P.G. Koutsoukos. 1992. The precipitation of calcium carbonate in artificial seawater at sustained supersaturation. *Environmental technology*, *13*(1), 73-80.

Rausis, K., Ćwik, A., and I. Casanova. 2020. Phase evolution during accelerated CO2 mineralization of brucite under concentrated CO2 and simulated flue gas conditions. *Journal of CO2 Utilization*, *37*, 122-133.

Rietveld, H. M. 1969. A profile refinement method for nuclear and magnetic structures. *Journal of applied Crystallography*, *2*(2), 65-71.

United States Environmental Protection Agency (USEPA). 2013. *Record of decision, Gowanus Canal Superfund Site, Brooklyn, Kings, County, New York*. September.

USEPA. 2017. *SW-846 Test Method 1315: Mass Transfer Rates of Constituents in Monolithic or Compacted Granular Materials using a Semi-Dynamic Tank Leaching Procedure.* Test Methods for Evaluating Solid Waste: Physical/Chemical Methods SW-846 Method 1315. Washington, DC. July.